Proceedings of the ASME 2018 International Mechanical Engineering Congress and Exposition
IMECE2018
November 9-15, 2018, Pittsburgh, PA, USA

IMECE2018-86549

DOWNWIND TWO-BLADED WIND TURBINE AERODYNAMIC PERFORMANCE EVALUATION IMPLEMENTING ACTUATOR LINE MODEL

Sebastian Henao*
Mechanical Engineering Department
National University of Colombia
Medellín, Colombia
Email: sehenaoga@unal.edu.co

Aldo G. Benavides
Mechanical Engineering Department
National University of Colombia
Medellín, Colombia
Email: agbenavidesm@unal.edu.co

Omar D. López
Mechanical Engineering Department
Los Andes University
Bogotá, Colombia
Email: od.lopez20@uniandes.edu.co

ABSTRACT

The current trend in the wind power market is to develop large diameter rotors in order to maximize the power extraction from the wind. Those rotors exhibit issues related to blade deflection and structural integrity that can be mitigated implementing design variations that were present on the early wind turbine designs, such as rotors with less than three blades located behind the tower in downwind configuration. This work assesses the aerodynamic performance of a downwind two-bladed wind turbine based on CFD simulations coupled with the Actuator Line Model (ALM). This design is compared with the MEXICO project upwind three-bladed wind turbine, for which experimental data is available. The simulations showed good agreement with measurements especially upstream the rotor and for higher inlet velocities. Furthermore, the downwind configuration was successfully modeled using ALM and the performance prediction of the turbines was physically accurate since realistic variations were obtained between the evaluated wind turbines and none of their performance coefficients exceeded Betz theoretical limit.

1 INTRODUCTION

Wind turbines have revolutionized the energy market, providing a sustainable and efficient means for electrical power generation. This technology has become a promising alternative to satisfy the growing global energy demands, for which it is paramount to maximize the extraction of power from the wind. Several wind turbines designs have been tested throughout the last decades, among which the large horizontal axis wind turbines have proved to be the most suitable for large scale power generation. Regarding the number of blades, at the early years of wind power technology, two-bladed rotor turbines were preferred; nowadays the three-bladed model is the most common type of wind turbine given that those extract higher amounts of power at lower specific tip-speed ratios. However, two-bladed wind turbines offer a wider range of operation, which reflects on a lower incidence of tip-speed variations over the extracted power [1]. The downwind configuration, i.e. where the rotor is located behind the tower, was also present on the early wind turbine designs but it was replaced by the upwind configuration, which in addition to the tree-bladed model, was argued to perform at lower noise levels with improved power extraction [1]. The aerodynamic performance of wind turbines depends on wind velocity and rotor diameter, even though, just the latter is a parameter that can be adjusted during the turbine design. Therefore, the current trend is to design large diameter rotors; however, those massive rotors exhibit issues related to blade deflection and structural integrity. This can be mitigated by getting back to the early two-bladed downwind model that provides flexibility on blade design and rotor weight, especially for high speed rotors [1]. Nevertheless, the performance of this design variation is not well documented on the literature.

On the other hand, as the requirements for wind turbines increase, it is necessary to develop more reliable tools to aid their design providing accurate wake, loads and performance predictions. In such an endeavor, several engineering models have been proposed, ranging from simplified aerodynamic models based on

*Address all correspondence to this author.

the Blade Element and Momentum theory (BEM), to more complex models, such as CFD methods, which require large amounts of computational resources [2]. It is also necessary to provide experimental measurements to assess the accuracy of such engineering models, for which both full-scale and laboratory models have been evaluated. For instance, the Model Experiments in Controlled Conditions (MEXICO) project developed by the Energy Research Center of the Netherlands et al. in 2007 [3] provide detailed aerodynamic and load measurements on an upwind three-bladed wind turbine model, which was tested in a large wind tunnel. This experimental campaign was developed as a complement to the NREL NASA Ames Unsteady Aerodynamic Experiment (UAE) database registered by the U.S. National Renewable Energy Laboratory (NREL) in 2001 [4], where the performance of a two-bladed wind turbine both in upwind and downwind configurations was evaluated.

At first, the aim of the current work was to numerically reproduce the experimental wake measurements taken on the MEXICO project. The numerical simulations were carried out using the Actuator Line Model (ALM) [5, 6] implemented in an open-source CFD package. Then, the work focused on simulating the operation of a downwind two-bladed wind turbine design obtained from modifying the MEXICO turbine. The rotor diameter and operating conditions of the turbines were kept constant so just the rotor position and number of blades varied between models.

The Actuator Line Model is a simplified method for computing the flow field around wind turbines that combines a three-dimensional Navier-Stokes solver with a so-called actuator line technique, in which body forces are distributed radially along rotating lines representing the blades of the wind turbine. Those lines are denoted as actuator lines and are composed by actuator points, where the loading is determined iteratively using a blade-element approach and tabulated airfoil data. Then, that loading is projected onto the computational domain representing the flow field, which consists of a single hexahedral mesh. Given the simplified geometric representation, there is no need to account for rotational meshes nor to solve for the boundary layer on the surface of the blades. The method was first proposed by Sørensen and Shen [5] in 2002 and was tested by simulating a commercial 500 kW wind turbine with a rotor diameter of 41 m. The computed power production was found to be in good agreement with measurements, and the flow field around the rotor was well represented. The first version of the method was formulated in vorticity-velocity variables, but in 2003, Mikkelsen [6] reformulated it in pressure-velocity variables and proposed a more accurate model for distributing the forces on the lines. Based upon this, several studies have been carried out in order to replicate the experimental measurements of wind turbines. For instance, Troldborg et al. [7] used ALM to study the flow field around two commercial rotors whose diameters were 30.56 m and 40.04 m. They were able to obtain detailed information about the wake development including vortex properties and turbulence characteristics. Matiz [8] used the method to simulate the operation of the NREL UAE Phase VI wind turbine including both the 10 m diameter rotor and tower, and found that the method is fully capable of simulating the aerodynamics of the tower and can account for its incidence on the turbine performance. Also, control parameters such as mesh resolution, actuator point distribution and the shape of the force projection have been assessed in order to conclude about their incidence on the simulations results [7–10].

Regarding the MEXICO Project, several studies have been carried out in order to process, analyze and numerically replicate the experimental data for the evaluated wind turbine [11,12]. There is no detailed analysis reported for this turbine implementing ALM; however, it has been done with other computational approaches, such as fully three-dimensional CFD simulations. For instance, Bechmann et al. [13] investigated the MEXICO rotor through 3D steady-state fully turbulent simulations in order to reproduce the rotor wake. Even though their simulation results and experimental data compared well, it was not clear whether the wind tunnel geometry significantly influenced the turbine performance. To further investigate this issue, Réthoré et al. [14] carried out CFD simulations including the wind tunnel. They found that the effect of the wind tunnel over the region of comparison of the wake was not significant since the main effects are noted outside of the region where velocity measurements were taken. Both studies show that, even though the wake is well predicted by the numerical simulations, it does not hold for the forces on the blades, which are overestimated with respect to measurements. The authors argue that this could potentially indicate an underestimation of the blade loadings measurements.

The next section provides a detailed description of the assessed wind turbines, the available experimental data and a description of the simulations performed. Following, the numerical simulation results are presented along with an analysis of their agreement with the experimental measurements and a comparison of the performance of both wind turbines.

2 METHODS

A set of wind turbine simulations were performed implementing the ALM in order to compute the wake around the turbines and to assess their performance. The base case aimed to reproduce the experimental wake measurements taken during the MEXICO project for a three-bladed upwind 4.5 m diameter rotor, for which mesh independence was assessed and the optimal ALM input parameters were defined. Based upon this turbine model, an alternative two-bladed downwind wind turbine model was numerically evaluated. Simulations were performed using the open-source Navier-Stokes solver OpenFOAM coupled with the ALM package SOWFA developed by NREL [15].

2.1 MEXICO Project

The Model Experiments in Controlled Conditions (MEXICO) was an experimental campaign where a database of detailed aerodynamic and load measurements on a wind turbine model was created. The wind tunnel experiment was executed in the Large Scale Low Speed Facility of the German Dutch Wind tunnel Organization (DNW) in an open section of $9.5 \times 9.5\ m^2$. The measurements covered three operational tip-speed ratios, many blade pitch angles, three yaw misalignment angles and unsteady cases in the form of pitch and rotor speed ramps [11]. The most important feature of the measurements is the flow field mapping using Particle Image Velocimetry (PIV) from about one diameter upstream to one diameter downstream, even though, global forces were not measured on the rotor [13]. Those flow field measurements allowed to validate the accuracy of the conducted ALM simulations.

The MEXICO wind turbine main geometric characteristics are shown in Table 1. Details about the blades chord and twist distribution can be found in [13]. The turbine was designed for an optimum tip-speed ratio of 6.7, reached at a tunnel velocity of $15\ m/s$.

TABLE 1: MEXICO WIND TURBINE GEOMETRIC CHARACTERISTICS [13]

Rotor diameter	$4.5\ m$
Number of blades	3
Rotor configuration	Upwind
Tower height	$5\ m$
Tower diameter	$0.5\ m$
Tower clearance	$3\ m$

Each one of its blades is composed of three airfoil references and were numerically milled from aluminum [11]. The blade airfoil distribution is detailed in the Table 2. Data regarding transition regions between airfoils was not available, so those were handled as discontinuities on the simulations. The 2D airfoil data used can be found in references [16,17]. It consisted of raw drag and lift coefficients as a function of the angle of attack. No correction for the three-dimensional effects on the flow was taken into account. The average drag and lift coefficients used for the tower are reported in [18].

From the available experimental data recorded for several operating conditions, three cases of the run 11 have been selected for which PIV measurements were taken. Each one of those cases are identified with a single data point number in the MEXICO database and have been selected in such way that only the wind tunnel speed varies among them. Each data point consists of 100 PIV measurements taken in about 40 seconds at a frequency of 2.4 Hz [3]. Table 3 exposes the operating conditions that were investigated.

TABLE 2: MEXICO WIND TURBINE BLADES AIRFOIL DISTRIBUTION [13]

Radius $[m]$	**Blade** %	**Airfoil**
0.450 - 1.125	20% - 50%	DU91-W2-250
1.125 - 1.575	50% - 70%	RISØE-A1-21
1.575 - 2.250	70% - 100%	NACA 64-418

TABLE 3: OPERATING CONDITIONS [13]

	Data point		
Variable	92	93	95
Wind tunnel speed	$10\ m/s$	$15\ m/s$	$24\ m/s$
Tip-speed ratio	10	6.7	4.2
Angular velocity	425.5 RPM ($44.44\ rad/s$)		
Pitch angle	$-2.3°$		
Yaw angle	$0°$		

The experimental measurements used consisted of axial velocity measurements taken both upstream and downstream of the rotor using the PIV technique. The measurement tower was mounted on a traversing mechanism which made it possible to take measurements in an axial range of about $10\ m$ and a radial range of about $1.2\ m$. Further details about the measurement process and the PIV technique used can be found in [3,13]. The (x,r) coordinate system shown in the MEXICO wind turbine schematic (Fig. 1), the rotor diameter (D) and rotor radius $(R = D/2)$ are employed to describe the locations at which measurements were taken. The axial traverses, i.e. perpendicular to the rotor plane and parallel to the x direction, were taken in 12 fixed axial points ranging from $4.325\ m$ upstream the rotor $(x/D = -0.96)$ to $5.725\ m$ downstream $(x/D = 1.27)$ at the fixed heights of $1.374\ m$ $(r/R = 0.61)$ and $1.845\ m$ $(r/R = 0.82)$ measured from the center of the rotor upward. However, Schepers and Snel [3] reported that the measurements at $r/R = 0.61$ do not compare well with the theoretical estimates due to the release of a trailing vortical structure at this position. Therefore, only the measurements at $r/R = 0.82$ were taken into account. The radial traverses, i.e. parallel to the rotor plane and to the

r direction, were taken at 4 fixed axial positions ranging from $x/D = -0.56$ to $x/D = 1.04$. The radial locations covered were between the heights of 1.2 m ($r/R = 0.48$) and 2 m ($r/R = 0.8$), also measured from the center of the rotor upward. Experimental measurements are shown, along with simulation results, in section 3.

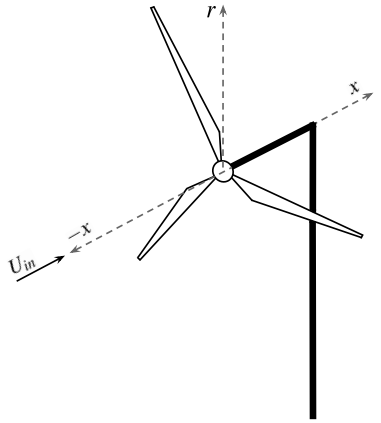

FIGURE 1: MEXICO WIND TURBINE SCHEMATIC

2.2 Modified Wind Turbine

The MEXICO wind turbine simulation was modified to assess the performance of a two-bladed downwind wind turbine and further compare it against the base turbine. Table 4 presents the geometric characteristics of the modified wind turbine. Just the number of blades and location of the rotor with respect to the tower was modified. Moreover, all the operating conditions were kept as shown in Table 3 for the simulations carried out with the modified turbine.

TABLE 4: MODIFIED WIND TURBINE GEOMETRIC CHARACTERISTICS [13]

Rotor diameter	4.5 m
Number of blades	2
Rotor configuration	Downwind
Tower height	5 m
Tower diameter	0.5 m
Tower clearance	3 m

2.3 Numerics

2.3.1 Governing Equations Given that the wind turbine maintains a constant angular velocity, at the tip of the blades the Reynolds number is maximized while maintaining a Mach number below 0.3 for the constant tip-speed of 100 m/s as stated by Snel et al. [11]. Therefore, the air flow was assumed to be in a fully incompressible and turbulent regime and the Reynolds-averaged Navier-Stokes equations for viscous, unsteady, turbulent, three-dimensional and incompressible fluid flow in rectangular coordinates were solved using the Finite Volume Method (FVM) [19]. The fluid properties were assumed to be constant so the continuity and momentum equations are decoupled from the energy equation. Also, given the incompressible flow regime, the body force due to gravity was not taken into account. The analyzed continuity and momentum equations in tensor notation are shown in Eqns. 1 and 2, respectively.

$$\frac{\partial \bar{u}_i}{\partial x_i} = 0 \tag{1}$$

$$\rho\left[\frac{\partial \bar{u}_i}{\partial t} + \bar{u}_j\frac{\partial \bar{u}_i}{\partial x_j}\right] = -\frac{\partial P}{\partial x_i} + \frac{\partial}{\partial x_j}\left[\tau_{ij} - \rho\overline{u_i' u_j'}\right] + \rho f_i \tag{2}$$

Where $\bar{u}$ denotes the mean velocity, ρ the fluid density, P the mean pressure field, τ the mean viscous stress tensor, $\rho\overline{u_i' u_j'}$ the Reynolds stresses and f_i the external body forces applied into the system which, for instance, represent the loadings on the blades. The two equation $k-\omega$ SST turbulence model was used to approximate the turbulent flow as proposed by Matiz [8] and Bechmann et al. [13].

The ALM couples with the Navier-Stokes equations through the computation of the body forces that account for the blade loadings. At first, each blade represented by an actuator line, is divided into a set of actuator points where the aerodynamic loads are computed using a basic BEM approach combined with the tabulated two-dimensional airfoil characteristics. This will give a two-dimensional force that accounts for the lift and drag on the blade, which is denoted f_i^{2D}. Then, the computed aerodynamic force is projected onto the flow field, which is required to be smoothly distributed over several cells in order to avoid singular behavior. This is accomplished, as proposed by Søresen and Shen [5], by using a Gaussian distribution. Eqn. 3 defines the magnitude of a local force projection on the flow field of a given actuator point.

$$f_i = f_i^{2D}\frac{1}{\varepsilon^3\pi^{\frac{3}{2}}}\exp[-(r/\varepsilon)^2] \tag{3}$$

Here, r is the distance between the point in the flow field and the actuator point on the blade to which f_i^{2D} is associated. This distance is controlled by the ε parameter, denoted the Gaussian radius [9], which specifies the radius of the body force projection function. Further details about the body force computation procedure can be found in [5–8] and the incidence of the ε parameter on the simulation results was carefully studied in [7–9]. Here, the recommendation made by Matiz [8] to set ε equal to the chord of the blade at the $r/R = 0.95$ section was implemented and the Gaussian radius was set to $\varepsilon = 0.1$.

Regarding the time discretization of the simulation, both Matiz [8] and Troldborg et al. [7] proposed to define it in such way that the movement of the blade tip during one time step did not exceed one grid spacing. Therefore, Troldborg et al. [7] proposed that the number of time steps per revolution should not be lower than 200 in order to obtain accurate results. This was the selected criterion, which translated into a time step of $7\text{x}10^{-4}$ s. This was found to be more restrictive than the Courant number criterion [8], which requires a non-dimensional quantity related to free stream velocity, grid resolution and simulation time step to be lower than 1. However, the highest Courant number found among all the simulations performed was equal to 0.17.

2.3.2 Computational Domain The computational domain used consists of a single hexahedral block as shown in Fig. 2. The (X,Y,Z) coordinate system was defined in a way that the X direction is parallel to the flow, whereas the Z direction is parallel to the tower, making the YZ plane parallel to the rotor. This coordinate system belongs to the simulation itself and should not be confused with the (x,r) coordinate system used to describe the experimental measurements taken at the MEXICO project. The domain dimensions (Table 5) were chosen following the recommendations made by Matiz [8], which were proven to be large enough to reduce the effect of the boundaries on the velocity field in the rotor zone.

TABLE 5: COMPUTATIONAL DOMAIN SIZE

Direction name	Coordinate	Size	Length $[m]$
East	X	10D	45
North	Y	5D	22.5
Up	Z	5D	22.5

Regarding the location of the turbine, the tower base location for both wind turbines was defined at the point $P = (15, 11.25, 0)$. From there, accounting for the tower clearance, the rotor is located 3 m upstream for the MEXICO wind turbine cases and downstream for the two-bladed wind turbine cases.

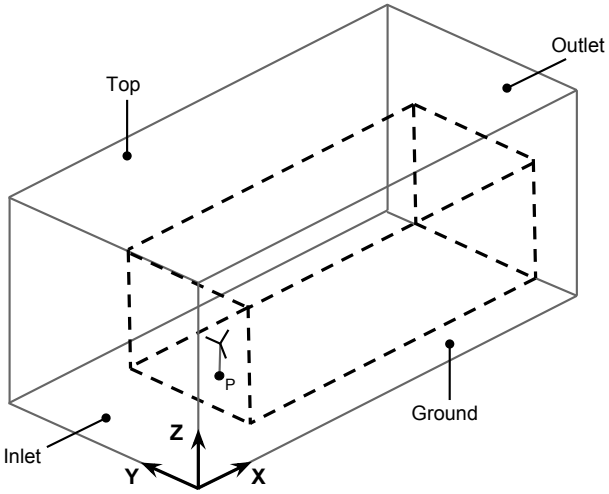

FIGURE 2: COMPUTATIONAL DOMAIN

The main advantage of the ALM is that a very simple three-dimensional mesh is used since no complex geometry needs to be meshed. Therefore, the mesh consists entirely of hexahedral cells. Several refinements have been conducted in the domain in order to provide finner cells in the vicinity of the turbine, where higher gradients are expected. It was accomplished by setting grading factors towards the box represented by the dashed lines in Fig. 2, which defines the most refined region of the domain. Table 6 shows the dimensions of this region. Moreover, inside of this region, the cells are finner as they approach the turbine and become coarser as they approach the outlet of the domain. A grading factor towards the ground of the domain was also defined in order to account for the boundary layer.

TABLE 6: REFINED REGION SIZE

Coordinate	Size	Length $[m]$
X	7.5D	33.75
Y	3D	13.5
Z	3D	13.5

The boundary conditions applied on the domain are shown in Table 7. Inlet velocity U_{in} depends on the wind tunnel speed, whereas a no slip boundary condition was defined at the ground. The turbulence kinetic energy k is estimated as proportional to the square of U_{in} and the turbulence intensity I, which was set to 1% due to the uncertainties in the real turbulence magnitude. The turbulence frequency ω depends on k, an empirical non-dimensional constant $C_\mu = 0.09$ and the turbulence length

$L = 0.07D_H = 0.16$, where D_H denotes the hydraulic diameter computed for the domain cross section. The outlet pressure was set to the atmospheric pressure and in the remaining faces zero normal gradient boundary conditions were set. In addition, it is noted that the ALM does not require boundary conditions defined near the turbine given the simplified geometric representation used.

TABLE 7: BOUNDARY CONDITIONS

Boundary	U	P	k	ω
Inlet	U_{in}	$\frac{\partial P}{\partial x} = 0$	$\frac{3}{2}(U_{in}I)^2$	$\frac{k^{1.5}}{C_\mu L}$
Outlet	$\frac{\partial U}{\partial x} = 0$	P_{atm}	$\frac{\partial k}{\partial x} = 0$	$\frac{\partial \omega}{\partial x} = 0$
Ground	0	$\frac{\partial P}{\partial z} = 0$	$\frac{\partial k}{\partial z} = 0$	$\frac{\partial \omega}{\partial z} = 0$
Top	$\frac{\partial U}{\partial z} = 0$	$\frac{\partial P}{\partial z} = 0$	$\frac{\partial k}{\partial z} = 0$	$\frac{\partial \omega}{\partial z} = 0$
Sides	$\frac{\partial U}{\partial y} = 0$	$\frac{\partial P}{\partial y} = 0$	$\frac{\partial k}{\partial y} = 0$	$\frac{\partial \omega}{\partial y} = 0$

The mesh was refined several times by increasing the number of cells in the domain. Table 8 lists the cell divisions in each direction and the total number of cells for each of the refinement steps performed to verify the grid independence of the solution.

TABLE 8: MESH REFINEMENT STEPS

	Cell divisions		
Direction	**Step 1**	**Step 2**	**Step 3**
X	100	150	180
Y	50	100	130
Z	50	100	130
Total cells	$2.5e5$	$1.5e6$	$3e6$

2.3.3 Numerical Simulations The numerical simulations were performed using OpenFOAM coupled with the Simulator For Wind Farm Application (SOWFA) developed by Churchfield et al. at NREL in 2012 [15]. The latter implements the ALM for the simulation of wind turbines and the former provides a Navier-Stokes three-dimensional solver.

All the simulations contained both the tower and the rotor. The mesh and the coordinate system of the domain were set according to the guidelines given by Churchfield et al. [15] and 50 actuator points were used to decompose each blade, for which geometric and aerodynamic properties were given. The total simulated time was of 2.1 s, resulting in 3000 time steps for each simulation.

The simulations were performed in a set of runs where the inlet velocity, the mesh parameters and the turbine geometric characteristics were varied. Table 9 summarizes all the performed simulations. At first, the purpose was to validate the grid independence of the solution, for which the MEXICO wind turbine and the 10 m/s inlet velocity were used covering the three mesh refinement steps. Then, using the mesh for which convergence was obtained, two additional simulations were performed for the MEXICO rotor to cover the complete set of wind tunnel velocities for which experimental data is available. Finally, the downwind two-bladed (DTB) wind turbine was simulated using the three inlet velocities shown in Table 3 to directly compare its performance with the MEXICO wind turbine.

TABLE 9: SIMUTLATIONS RUNS SUMMARY

Run	**Turbine**	**Inlet velocity** $[m/s]$	**Mesh step**
1	MEXICO	10	1
2	MEXICO	10	2
3	MEXICO	10	3
4	MEXICO	15	2
5	MEXICO	24	2
6	DTB	10	2
7	DTB	15	2
8	DTB	24	2

3 RESULTS AND DISCUSSION

All eight cases listed in Table 9 were simulated and major findings are presented in this section. The analyzed quantities consist of wake and performance characteristics and are presented in the form of graphs and tables using non-dimensional coefficients. All the presented results related to the wake around the turbine were extracted for the last time step and no time averaging was conducted. Whereas for the wind turbine performance, the results were averaged in the time frame from 0.5 s to 2.1 s. All the results extracted from the simulation were translated into the coordinate system exposed on Fig. 1 so those can be directly compared against the available measurements. The following graphs represent experimental data using symbols whereas simulation results are represented using continuous and dashed lines.

3.1 Mesh Independence

To assess the grid dependence of the simulation results, three MEXICO wind turbine simulations were performed starting with a base mesh and two subsequent refinements. The simulations results were analyzed computing the axial induction (Eqn. 4) along the axial traverse for which experimental data is available. This parameter was selected as a means for evaluating the drop of axial velocity with a non-dimensional coefficient.

$$a = \frac{U}{U_{ref}} \tag{4}$$

Where U represents the axial velocity at a given point of the axial traverse and U_{ref} represents the reference velocity for each case. Hence, in order to obtain the samplings of U, velocity results in the X direction were extracted at several points along the axial traverse and averaged in a horizontal traverse defined at the fixed radial position $r/R = 0.82$, resembling the location and extension of the PIV sheet described by Schepers et al. [3] and Snel et al. [11].

For the mesh independence assessment, the three simulations were performed using the inlet velocity of 10 m/s and the reference velocity for computing the axial induction was obtained at the location $x/D = -0.96$. Simulation results and experimental data are shown in Fig. 3.

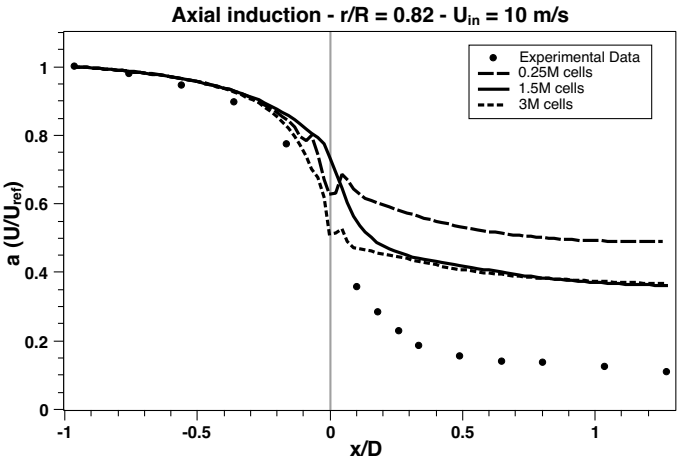

FIGURE 3: MESH INDEPENDENCE EVALUATION

Good agreement between simulation results and experimental measurements was found for the wake upstream the rotor for all the mesh refinement steps, even though it does not hold for the wake downstream. Furthermore, even for the last mesh refinement step, the simulation results are far from the experimental measurements downstream the rotor. However, the simulations results converge so the differences may not be related to mesh refinement. The second mesh refinement step was used as the default mesh for the subsequent simulations as the results variations with respect to the third mesh refinement step are low.

3.2 Experimental Data Validation

To further evaluate the difference between the experimental data and the simulation results evidenced in Fig. 3, two additional simulations were performed to cover the two remaining wind tunnel velocities shown in Table 3. The simulation results were compared with the axial and radial traverses for which wake measurements are available. Those traverses are computed as described in section 3.1, averaging at each of the x/D locations for the radial traverses. For computing the axial induction for the radial traverses, the velocity found in the location $x/D = -0.96$ at a height $r/R = 0.82$ was used as (U_{ref}) for all the curves shown within a figure.

Regarding the axial traverses (Fig. 4), it is seen that the simulations results for the wake downstream closely follow the experimental measurements as the inlet velocity increases, whereas the wake upstream compare well for all the analyzed velocities. Indeed, for the $U_{in} = 24$ m/s case, a really close agreement is found between measurements and simulations. Furthermore, for the remaining inlet velocities, the simulation results follow the same behavior as the experimental results; however, simulations predict higher axial induction downstream, which means lower velocity drops across the rotor, evidencing that a lower amount of power from the wind is being extracted. It is important to note that all the simulations were performed using the same mesh and geometry parameters and that the inlet velocity was the only parameter that varied among them.

The radial traverses for the three inlet velocities show a similar behavior with respect to the axial traverses. At first it is seen in Fig. 5 that good agreement between measurements and simulation was found at the x/D locations upstream the rotor, which also holds for the other two inlet velocities, with lower agreement in the case of $U_{in} = 15$ m/s (Fig. 6). Downstream the rotor the results were not as close to measurements as it was noted on the axial traverses analysis; however, the $U_{in} = 24$ m/s case also showed good agreement downstream (Fig. 7) despite the variations on the measurements. The worst scenario was observed for the $U_{in} = 15$ m/s case, where poor agreement was observed both upstream and downstream of the rotor.

Given that Bechmann et al. [13] performed fully three-dimensional CFD simulations of the MEXICO rotor and were able to obtain good agreement between measurements and simulations results for all the analyzed inlet velocities, errors in the wake measurements are not feasible. Hence, the exposed analysis evidences that the differences found in the wake prediction downstream the rotor are not related to grid dependency nor sim-

ulation setup issues but to the simplified rotor representation itself.

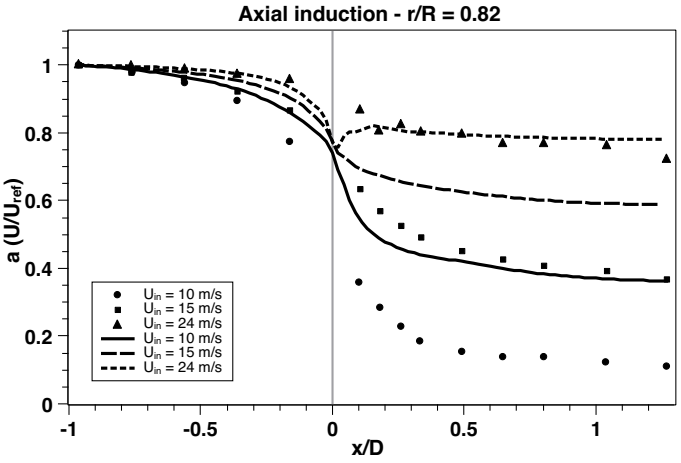

FIGURE 4: MEXICO WIND TURBINE AXIAL TRAVERSES COMPARISON

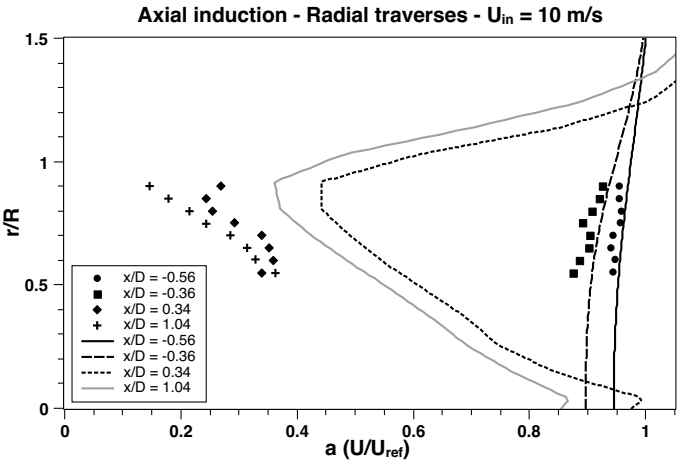

FIGURE 5: MEXICO WIND TURBINE RADIAL TRAVERSES COMPARISON - $U_{in} = 10\ m/s$

3.3 Downwind two-bladed turbine wake

Given that the downwind two-bladed turbine model was obtained from modifying the MEXICO turbine and that there are no reported measurements for this design variation, the accuracy of those simulations had to be assessed in a qualitative way. Therefore, the physical behavior of the wake is analyzed through the axial induction both in longitudinal and transverse directions.

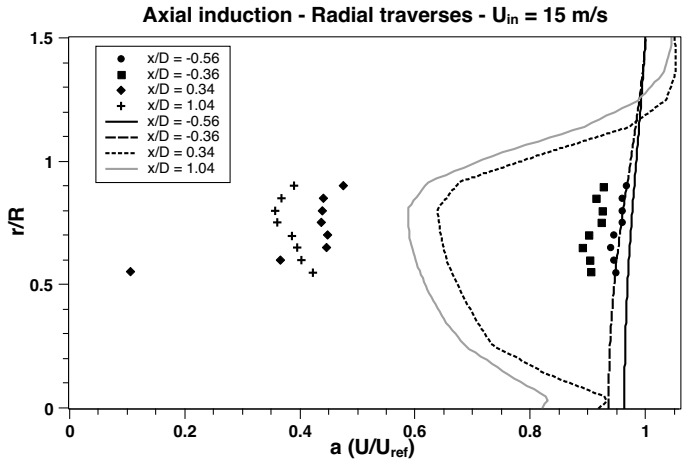

FIGURE 6: MEXICO WIND TURBINE RADIAL TRAVERSES COMPARISON - $U_{in} = 15\ m/s$

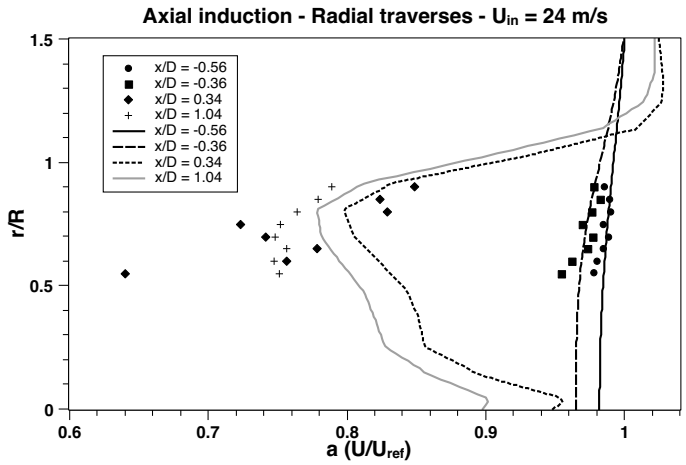

FIGURE 7: MEXICO WIND TURBINE RADIAL TRAVERSES COMPARISON - $U_{in} = 24\ m/s$

At first, Fig. 8 depicts the axial velocity profile for the downwind two-bladed wind turbine in a similar way to how the axial traverses were represented for the MEXICO turbine. Results are shown for a longitudinal plane that spans from $x/D = -0.96$ to $x/D = 1.27$ and that is located at a radial position of $r/R = -0.82$, where the tower effect can also be noted. The axial induction was computed using as reference velocity the axial velocity found at $x/D = -0.96$ upstream the rotor. Furthermore, the tower and rotor locations are represented to observe how the wake is modified with the presence of those two elements.

When the air flows through a downwind turbine, a drop in flow velocity is expected when it passes the tower before the ro-

tor. It is evidenced in Fig. 8 that the velocity drops suddenly at the tower location and that this drop continues at a slow pace but intensifies as the flow approaches the rotor location. Downstream of the tower, the wake behaves in a similar way as in the upwind configuration at a height of $r/R = 0.82$, where the tower effect downstream the rotor is not evidenced.

The axial velocity profile seen from a transverse plane located 0.5 m downstream the tower is shown in Fig. 9. The axial induction was also computed using as reference velocity the axial velocity found at $x/D = -0.96$. Here it is seen that the velocity drop on the tower also occurs in a transverse plane and that has small variations among the inlet velocities evaluated, as opposed to the velocity drop on the rotor, which has significant variations with the inlet velocity. Fig. 9 also shows the transverse length where the tower affects the flow, which extends further than the tower diameter.

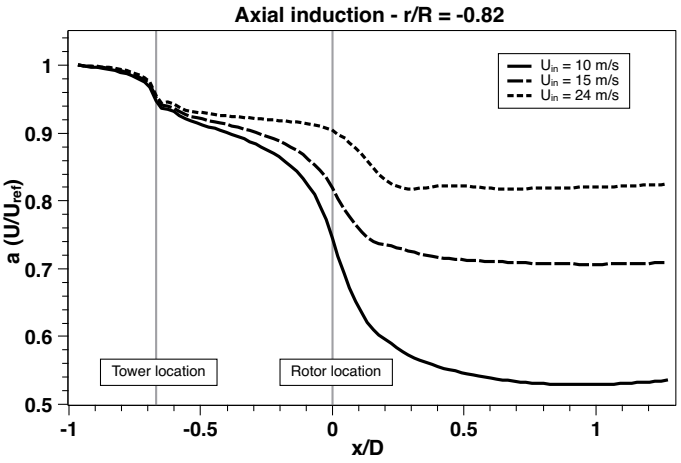

FIGURE 8: DOWNWIND TWO-BLADED WIND TURBINE AXIAL VELOCITY PROFILE

The results show that the downwind configuration of the turbine was accurately represented using the ALM since the physical behavior of the simulated flow agrees with expectations. However, experimental data is required in order to conclude about the accuracy of the simulation results.

3.4 Performance Evaluation

In order to assess the performance of the wind turbines analyzed, the power C_P and torque C_T coefficients were computed as functions of the inlet velocity both for the MEXICO and downwind two-bladed wind turbine (DTB). The results are shown in Table 10.

For the MEXICO wind turbine, is it seen that the highest power coefficient was obtained for the $U_{in} = 15\ m/s$, which is the inlet velocity related to the design tip-speed ratio. However,

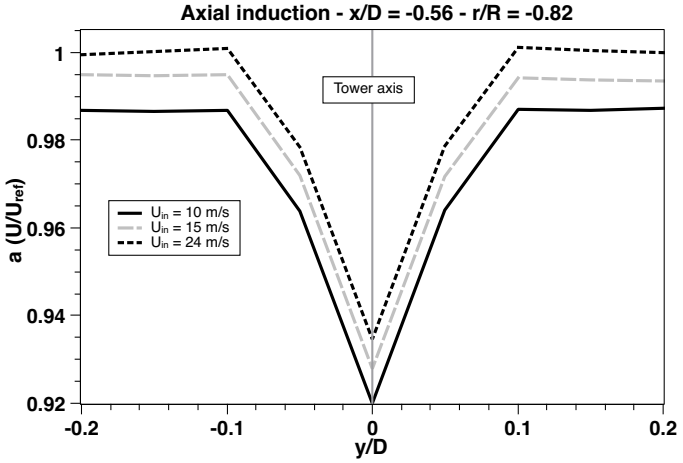

FIGURE 9: DOWNWIND TWO-BLADED WIND TURBINE RADIAL VELOCITY PROFILE

for the downwind two-bladed turbine, the highest power coefficient was registered for the $U_{in} = 10\ m/s$, which evidences that the design modifications of the base wind turbine reflected in a change of design tip-speed ratio. It is important to note that the angular velocity of the rotor and its diameter were kept constant so that the operational tip-speeds were not affected. Therefore, it is not feasible for the two-bladed model to extract the same or more power from the wind in comparison with the three-bladed model for those operational conditions. Indeed, this serves to validate the accuracy of the simulations. Furthermore, both turbines showed the lowest power coefficients for the highest inlet velocity and none of the simulations resulted in a power coefficient higher than the Betz limit, which would be physically incorrect. Regarding the torque coefficient, the obtained values were higher for the three-bladed model, which suggests its capability of extracting more torque from the wind given its higher number of blades.

TABLE 10: PERFORMANCE EVALUATION

	MEXICO		**DTB**	
$U_{in}[m/s]$	C_P	C_T	C_P	C_T
10	0.32	0.032	0.26	0.026
15	0.33	0.049	0.23	0.034
24	0.21	0.050	0.14	0.033

4 CONCLUSIONS

There is a growing need for computational tools that aid the design process of wind turbines providing accurate wake, loads and performance predictions. This paper focused on assessing the capabilities of the Actuator Line Model (ALM) to reproduce the experimental wake measurements for the MEXICO wind turbine and to predict the wake and performance of a downwind two-bladed wind turbine model. At first, the wind turbines characteristics, the numerical models and the simulations setup were described. Then, the results were presented covering the mesh independence evaluation, the experimental data validation and the wake and performance characteristics of the analyzed wind turbines.

Overall, it was shown that the ALM is fully capable of simulating the rotor and tower of the wind turbine in both upwind and downwind configurations and to properly reproduce the physical behavior of the wake. However, a good agreement was not found between experimental data and simulations results for low inlet velocities downstream the rotor. It was shown that the differences may not be associated with mesh dependency nor simulation setup issues. Therefore, the differences could indicate limitations of the model that need to be further addressed. The implementation of the method is fully dependent on several control parameters that were defined according to recommendations found in the literature for an accurate implementation of the ALM. Also, the open source package SOWFA coupled with OpenFOAM was used to perform the simulations using this method.

Regarding the downwind two-bladed wind turbine, it was noted that the wake performs as expected but that experimental measurements are needed to validate the results accuracy. The power coefficients obtained for this modified wind turbine were lower than those obtained for the base model given that the angular velocity of the rotor was kept constant. The highest power coefficient for the modified turbine was associated to the lower inlet velocity, which indicates that the design tip-speed ratio for the modified turbine is higher than the one for the three-bladed model. This suggests that two-bladed rotors need to perform at higher angular velocities in order to compensate the drop in the power extraction.

In conclusion, the present paper serves as evidence of the functionality of the ALM and its limitations in wind turbines wake and performance prediction. Future work should focus on assessing the dependence of the simulations results on the turbulence model used. Furthermore, the incidence of the number of actuator points used to represent the blades should also be evaluated, given that in the current analysis a fixed value was used based on suggestions found in the literature.

ACKNOWLEDGMENT

Thanks to professors Aldo G. Benavides and Omar D. Lopez for all their support during the development of the current project.

REFERENCES

[1] Jamieson, P., 2011. *Innovation in Wind Turbine Design*. John Wiley and Sons.

[2] Sørensen, J. N., 2011. "Aerodynamic aspects of wind energy conversion". *Annual Review of Fluid Mechanics,* ***43***(1), jan, pp. 427–448.

[3] Schepers, J. G., and Snel, H., 2007. Model experiments in controlled conditions - final report. Tech. rep., Energy Research Centre of the Netherlands (ECN).

[4] Hand, M. M., Simms, D. A., Fingersh, L. J., Jager, D. W., Cotrell, J. R., Schreck, S., and Larwood, S. M., 2001. Unsteady aerodynamics experiment phase VI: Wind tunnel test configurations and available data campaigns. Tech. rep., National Renewable Energy Laboratory, dec.

[5] Sørensen, J. N., and Shen, W. Z., 2002. "Numerical modeling of wind turbine wakes". *ASME Journal of Fluids Engineering,* ***124***(2), p. 393.

[6] Mikkelsen, R., 2003. "Actuator disc methods applied to wind turbines". PhD thesis, Technical University of Denmark.

[7] Troldborg, N., Srensen, J. N., and Mikkelsen, R. F., 2009. "Actuator line modeling of wind turbine wakes". PhD thesis, Technical University of Denmark.

[8] Matiz-Chicacausa, A., and Lopez, O. D., 2018. "Full downwind turbine simulations using actuator line method". *Modelling and Simulation in Engineering,* ***2018***, p. 10.

[9] Jha, P. K., Churchfield, M. J., Moriarty, P. J., and Schmitz, S., 2014. "Guidelines for volume force distributions within actuator line modeling of wind turbines on large-eddy simulation-type grids". *ASME Journal of Solar Energy Engineering,* ***136***(3), jan.

[10] Jha, P. K., and Schmitz, S., 2016. "Blade load unsteadiness and turbulence statistics in an actuator-line computed turbine–turbine interaction problem". *ASME Journal of Solar Energy Engineering,* ***138***(3), feb.

[11] Snel, H., Schepers, J. G., and Montgomerie, B., 2007. "The MEXICO project (model experiments in controlled conditions): The database and first results of data processing and interpretation". *Journal of Physics: Conference Series,* ***75***, jul.

[12] Schepers, J. G., Boorsma, K., Cho, T., Gomez-Iradi, S., Schaffarczyk, P., Jeromin, A., Shen, W. Z., Lutz, T., Meister, K., Stoevesandt, B., Schreck, S., Micallef, D., Pereira, R., Sant, T., Madsen, H. A., and Srensen, N. N., 2012. Analysis of mexico wind tunnel measurements. Tech. Rep.

12-004, Energy Research Centre of the Netherlands (ECN): Final report of IEA Task 29, Mexnext (Phase 1).
[13] Bechmann, A., Sørensen, N. N., and Zahle, F., 2011. "CFD simulations of the MEXICO rotor". *Wind Energy,* ***14***(5), jan, pp. 677–689.
[14] Réthoré, P.-E., Sørensen, N., Zahle, F., Bechmann, A., and Madsen, H., 2011. "MEXICO wind tunnel and wind turbine modelled in CFD". In 29th AIAA Applied Aerodynamics Conference, American Institute of Aeronautics and Astronautics.
[15] Churchfield, M., Lee, S., and Moriarty, P., 2012. Overview of the simulator for wind farm application (sowfa). Tech. rep., NREL.
[16] Bertagnolio, F., Sørensen, N. N., Johansen, J., and Fuglsang, P., 2001. Wind turbine airfoil catalogue. Tech. rep., Risø National Laboratory.
[17] Timmer, W., 2009. "An overview of NACA 6-digit airfoil series characteristics with reference to airfoils for large wind turbine blades". In 47th AIAA Aerospace Sciences Meeting including The New Horizons Forum and Aerospace Exposition, American Institute of Aeronautics and Astronautics.
[18] Anderson, J. D., 2010. *Fundamentals of Aerodynamics*. McGraw-Hill Education.
[19] Versteeg, H., and Malalasekera, W., 2007. *An Introduction to Computational Fluid Dynamics: The Finite Volume Method (2nd Edition)*. Pearson.